Title

THE EFFECT OF ELECTRODE PLACEMENT AND FINITE MATRIX CONDUCTIVITY ON THE PERFORMANCE OF FLOW-THROUGH POROUS ELECTRODES

Author

Trainham, James A.

Publication Date

1977-05-01

Submitted to Journal of the Electrochemical Society

UC-4
LBL-6260
Preprint c.1

THE EFFECT OF ELECTRODE PLACEMENT AND FINITE MATRIX CONDUCTIVITY ON THE PERFORMANCE OF FLOW-THROUGH POROUS ELECTRODES

James A. Trainham and John Newman

May 1977

Prepared for the U. S. Energy Research and Development Administration under Contract W-7405-ENG-48

DISCLAIMER

LBL-6260

The Effect of Electrode Placement and Finite Matrix Conductivity on the Performance of Flow-Through Porous Electrodes

James A. Trainham and John Newman

Materials and Molecular Research Division, Lawrence Berkeley Laboratory, and Department of Chemical Engineering, University of California, Berkeley, California 94720

May, 1977

Abstract

A one-dimensional model for flow-through porous electrodes is used to predict the effluent concentration as a function of matrix conductivity and electrode length for upstream and downstream placement of the counterelectrode and current collector relative to the fluid inlet to the working electrode. Two chemical systems are considered: 1) the removal of copper from sulfate solutions and 2) the removal of silver from thiosulfate solutions.

For an infinite matrix conductivity, the lowest effluent concentration is achieved when the counterelectrode is placed upstream to the fluid inlet of the working electrode. When the matrix conductivity is small, the lowest effluent concentration is still achieved for upstream placement of the counterelectrode; however, the optimum placement of the current collector depends on the chemical system and the value of the matrix conductivity that can be achieved in practice.

Calculations show that for downstream placement of the counterelectrode a limiting current distribution cannot be achieved (for electrode lengths of interest here). The most undesirable configuration for achieving a low effluent concentration when the matrix conductivity is low is when both the counterelectrode and current collector are placed downstream of the fluid inlet.

Distribution of potential, reaction rate, and electric driving force are presented for four different configurations: 1) upstream counterelectrode, downstream current collector, 2) downstream counter-electrode, upstream current collector, 3) upstream counterelectrode, upstream current collector and 4) downstream counterelectrode, downstream current collector.

Introduction

The model used in calculating the effects of counterelectrode placement and current collector placement (when the matrix conductivity is moderate) on the performance of flow-through porous electrodes was developed in a previous paper by the authors;[1] however, results were presented only for the effective matrix conductivity σ much greater than the effective solution conductivity κ.

To date, previous models for flow-through porous electrodes[2-6] have considered only an infinite matrix conductivity, and no comparisons have been made on the performance of these electrochemical reactors as a function of counterelectrode placement.

The purpose of this paper is to suggest the optimum electrode configuration for two cases: 1) when $\sigma >> \kappa$ we are concerned only with the upstream and downstream placement of the counterelectrode and 2) when $\sigma \approx \kappa$, placement of not only the counterelectrode is important but also the current collector placement must be considered. At least four geometric configurations are possible: 1) upstream counterelectrode, downstream current collector (UD), 2) downstream counterelectrode, upstream current collector (DU), 3) upstream counterelectrode, upstream current collector (UU) and 4) downstream counterelectrode, downstream current collector (DD), and are shown schematically in Figure 1. It should be noted that the direction of fluid flow through the counterelectrode is unimportant to the analysis to be considered as long as the products don't enter the electrode of interest.

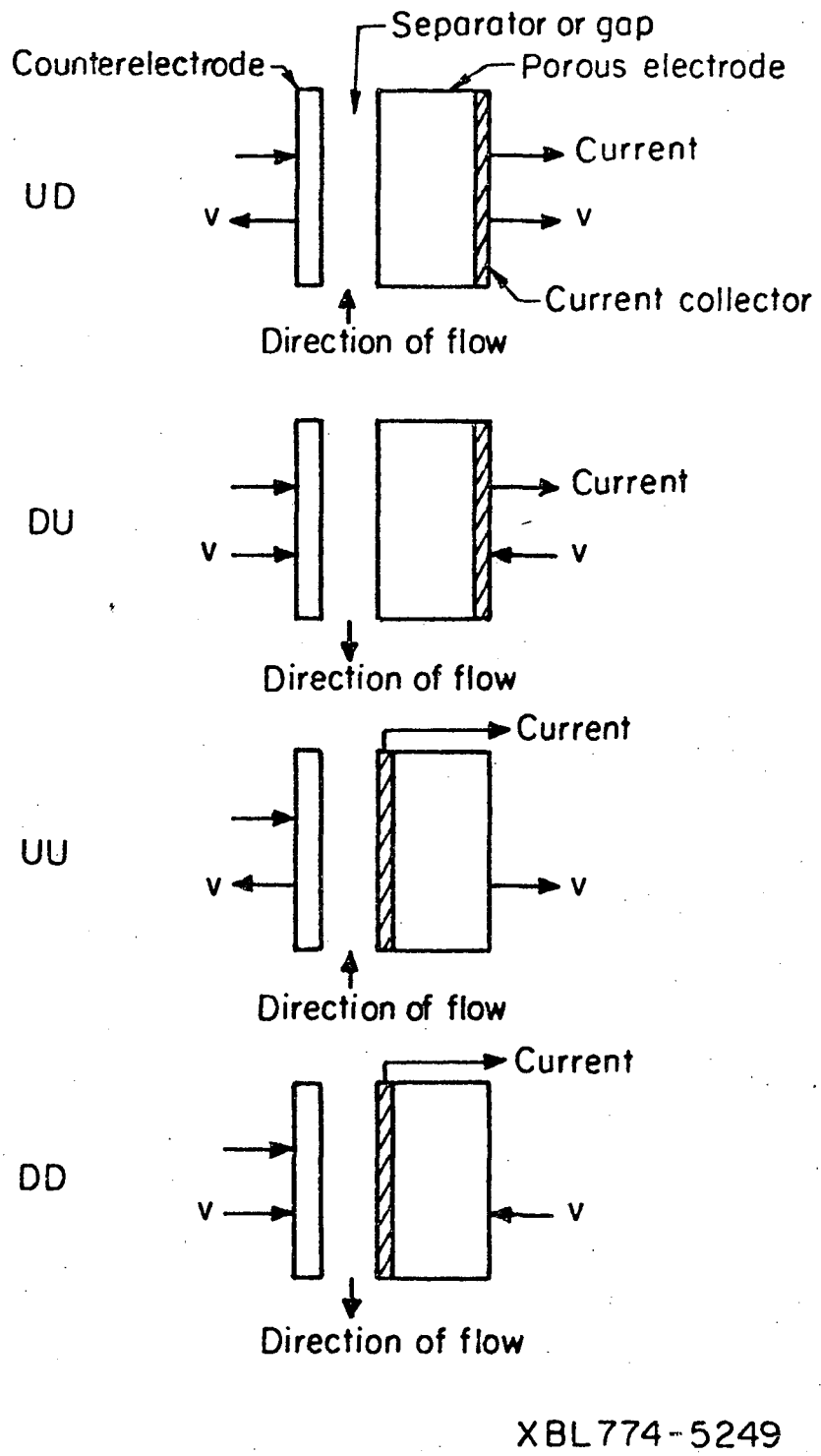

Figure 1. Various configurations of counterelectrode placement and current collector placement relative to the direction of the fluid flow.

Analysis

As mentioned earlier, calculations presented here are a direct application of a model for flow-through porous electrodes developed by the authors in a previous paper,[1] and therefore, detailed derivation of the governing equations will not be presented here.

For the removal of metal ions from dilute streams, the behavior of a flow-through porous electrode with parallel current and fluid flow as shown in Figure 1 can be described by two ordinary differential equations: one equation which describes the conservation of the metal-ion reactant

$$\frac{d\theta}{dy} = D' \frac{d^2\theta}{dy^2} - \frac{\theta - P_1 \exp\left[(\alpha_{aR}/\alpha_{cR} + 1)\eta'\right]}{1 + \exp(\eta')} , \qquad [1]$$

and one charge balance equation

$$\frac{d^2\eta'}{dy^2} = P_2 \left\{ P_3 \exp(-\alpha_{cS}\eta'/\alpha_{cR}) \left[1 - P_4 \exp\left(\frac{\alpha_{aS} + \alpha_{cS}}{\alpha_{cR}} \eta' \right) \right] + \frac{\theta - P_1 \exp\left[(\alpha_{aR}/\alpha_{cR} + 1)\eta'\right]}{1 + \exp(\eta')} \right\}, \qquad [2]$$

where θ is the reactant concentration divided by its value upstream in the feed, η' is the dimensionless local overpotential defined by

$$\exp(\eta') = - \frac{nFk_m c_{Rf}}{s_R i_{oR,ref}} \exp(\alpha_{cR} F\eta/RT) , \qquad [3]$$

and the reactor coordinate x was made dimensionless by

$$y = x\, a\, k_m/v = x\alpha \ . \qquad [4]$$

Equation 1 describes the conservation of the metal-ion reactant and states that convection is balanced by axial diffusion and dispersion, and the rate of disappearance of the metal ions due to electrochemical reaction at the matrix-solution interface. Mass transfer limitations are included by introducing an average mass-transfer coefficient k_m (see dimensionless parameter defined below) and eliminating the wall concentration of the metal-ion reactant.

The charge balance equation utilizes Ohm's law in both the matrix and solution phases and states that a change in the total current at any point within the electrode $(d^2\eta'/dy^2)$ is due to the rates of the side reaction and the main reaction. The term for the rate of the main reaction is the same in equations 1 and 2. The side reaction is characterized by its rate at the half-wave potential of the main reaction.

The dimensionless parameters in equations 1 and 2 are defined as follows:[1]

$$D' = (D_R + D_a)ak_m/v^2 \ ,$$

$$P_1 = \left(-\frac{s_R i_{oR,ref}}{nFk_m c_{Rf}}\right)^{1+\alpha_{aR}/\alpha_{cR}} \ ,$$

$$P_2 = \frac{\alpha_{cR} nF^2 v^2 c_{Rf}}{s_R a k_m RT}\left(\frac{1}{\kappa} + \frac{1}{\sigma}\right) \ ,$$

$$P_3 = - \frac{s_R i_{oS,ref}}{nFk_m c_{Rf}} e^{\alpha_{cS} F\Delta U/RT} \left(- \frac{nFk_m c_{Rf}}{s_R i_{oR,ref}} \right)^{\alpha_{cS}/\alpha_{cR}} ,$$

$$P_4 = \left(- \frac{s_R i_{oR,ref}}{nFk_m c_{Rf}} \right)^{\frac{\alpha_{aS}+\alpha_{cS}}{\alpha_{cR}}} \exp \left[-(\alpha_{aS} + \alpha_{cS}) \Delta UF/RT \right] . \qquad [5]$$

Boundary Conditions

Before equations 1 and 2 can be solved simultaneously for θ and η', four boundary conditions are required for each electrode configuration shown in Figure 1. For θ the following conditions were used

$$\theta - D' \frac{d\theta}{dy} = 1 \quad \text{at} \quad y = 0 ,$$

and

$$\frac{d\theta}{dy} = 0 \quad \text{at} \quad y = \alpha L , \qquad [6]$$

which are the Danckwerts,[7] Wehner-Wilhelm[8] conditions when axial diffusion and dispersion are included. The conditions on η' depend on electrode configuration and may be determined from Ohm's law

$$\frac{d\eta}{dx} = \frac{d(\Phi_1 - \Phi_2)}{dx} = - \frac{i_1}{\sigma} + \frac{i_2}{\kappa} , \qquad [7]$$

and are tabulated in Table 1. The dimensionless parameters P_5 and P_6 which arise in the analysis are related to P_2 :

$$P_5 = - \frac{\sigma P_2}{\sigma + \kappa} ,$$

Table 1. Current and potential boundary conditions for various electrode configurations.

Electrode Configuration	$i_1(0)$	$i_1(L)$	$i_2(0)$	$i_2(L)$	$d\eta/dx\|_{x=0}$	$d\eta/dx\|_{x=L}$	$d\eta'/dy\|_{y=0}$	$d\eta'/dy\|_{y=\alpha L}$
UD	0	$-i$	$-i$	0	$-i/\kappa$	i/σ	$P_5 I^*$	$-P_6 I^*$
DU	i	0	0	i	$-i/\sigma$	i/κ	$P_6 I^*$	$-P_5 I^*$
UU	i	0	$-i$	0	$-i\left(\frac{1}{\sigma}+\frac{1}{\kappa}\right)$	0	$-P_2 I^*$	0
DD	0	$-i$	0	i	0	$i\left(\frac{1}{\sigma}+\frac{1}{\kappa}\right)$	0	$P_2 I^*$

and

$$P_6 = - \frac{\kappa P_2}{\sigma + \kappa} , \qquad [8]$$

so that

$$-P_2 = P_5 + P_6 . \qquad [9]$$

The total current density i to the reactor was made dimensionless with the limiting current density that would exist if all the reactant in the feed were completely reacted:

$$I^* = \frac{s_R i}{nFvc_{Rf}} . \qquad [10]$$

Now that all the boundary conditions for each electrode configuration have been specified, equations 1 and 2 can be solved simultaneously for θ and η' using Newman's method.[9]

The potential distribution in each phase $\Phi_1(x)$ and $\Phi_2(x)$ can then be obtained by solving equation 3 for η using the known distribution for η', along with the conservation of charge condition

$$\frac{di_1}{dx} = - \frac{di_2}{dx} , \qquad [11]$$

and substituting this condition into the derivative of equation 7

$$\frac{d^2\eta}{dx^2} = -\left(\frac{\kappa + \sigma}{\kappa\sigma}\right) \frac{di_1}{dx} , \qquad [12]$$

then finally substituting the derivative of Ohm's law for the matrix phase into equation 12 to yield

$$\frac{d^2\eta}{dx^2} = \frac{\kappa + \sigma}{\kappa} \frac{d^2\Phi_1}{dx^2} . \qquad [13]$$

Equation 13 may be integrated twice to yield an expression for Φ_1 :

$$\Phi_1 = \frac{\kappa}{\kappa + \sigma} (\eta + C_1 x + C_2) . \qquad [14]$$

The value of C_1 for the various configurations is obtained from the derivative of equation 14 using the values of i_1 and $d\eta/dx$ at the boundaries found in Table 1. The value of C_2 is then obtained by specifying $\Phi_1 = 0$ at the current collector and using a known value of η at the appropriate boundary. Table 2 summarizes the results for $\Phi_1(x)$ for the various configuration; $\Phi_2(x)$ is simply obtained by subtracting $\eta(x)$ from $\Phi_1(x)$.

Chemical Systems

For the calculations to be presented, two different chemical systems (copper removal from sulfate solutions[11] and silver removal from thiosulfate solutions[10]) are used to illustrate the effects of counterelectrode placement and current collector placement (when the matrix conductivity is finite) on electrode performance. The purpose of presenting results for two different chemical systems is to obtain reasonable values for the model parameters so that a valid comparison of electrode performance can be made when the side reaction

Table 2. Matrix potential distribution for various electrode configurations.

Electrode Configuration	Matrix Potential Distribution $\Phi_1(x)/\left(\frac{\kappa}{\kappa + \sigma}\right)$
UD	$\eta(x) - \eta(L) + \frac{i}{\kappa} L(x/L - 1)$
DU	$\eta(x) - \eta(0) - \frac{i}{\kappa} x$
UU	$\eta(x) - \eta(0)$
DD	$\eta(x) - \eta(L)$

is substantial (as for silver removal from thiosulfate solutions[10]) and when it is small (as for the copper recovery process[11]).

Figure 2 compares model calculations to the data of Van Zee and Newman[10] for silver removal from thiosulfate solutions using a porous carbon electrode. The quantities I and VOP are the total current to the reactor and the potential of the cathode current collector relative to a saturated calomel reference electrode placed in the effluent stream, respectively. The experimental effluent silver concentration (in mg/ℓ) are shown as the numbers below each curve corresponding to the open circles 0 . The numbers above each curve correspond to the solid dots • and are the calculated values of the effluent silver concentration (in mg/ℓ).

A similar model fit to the data of Bennion and Newman[11] for copper removal can be found in reference 1. Values of the parameters used to fit the data in reference 1 and in Figure 1 are given in Table 3.

Four parameters were adjusted to obtain agreement between calculated and experimental values in Figure 1: one value of the exchange current density for the main reaction (silver deposition from thiosulfate solutions), assumed to be the electrode reaction[12]

$$Ag(S_2O_3)_2^{3-} + e^- \rightarrow Ag + 2S_2O_3^{2-} \quad , \qquad [15]$$

and has a standard electrode potential[12] $U^{\theta}_{Ag/Ag(S_2O_3)_2^{3-}} = 0.0164$ V ; one value of the exchange current density for the side reaction (the reduction of thiosulfate), which was assumed to be the following reaction[10]

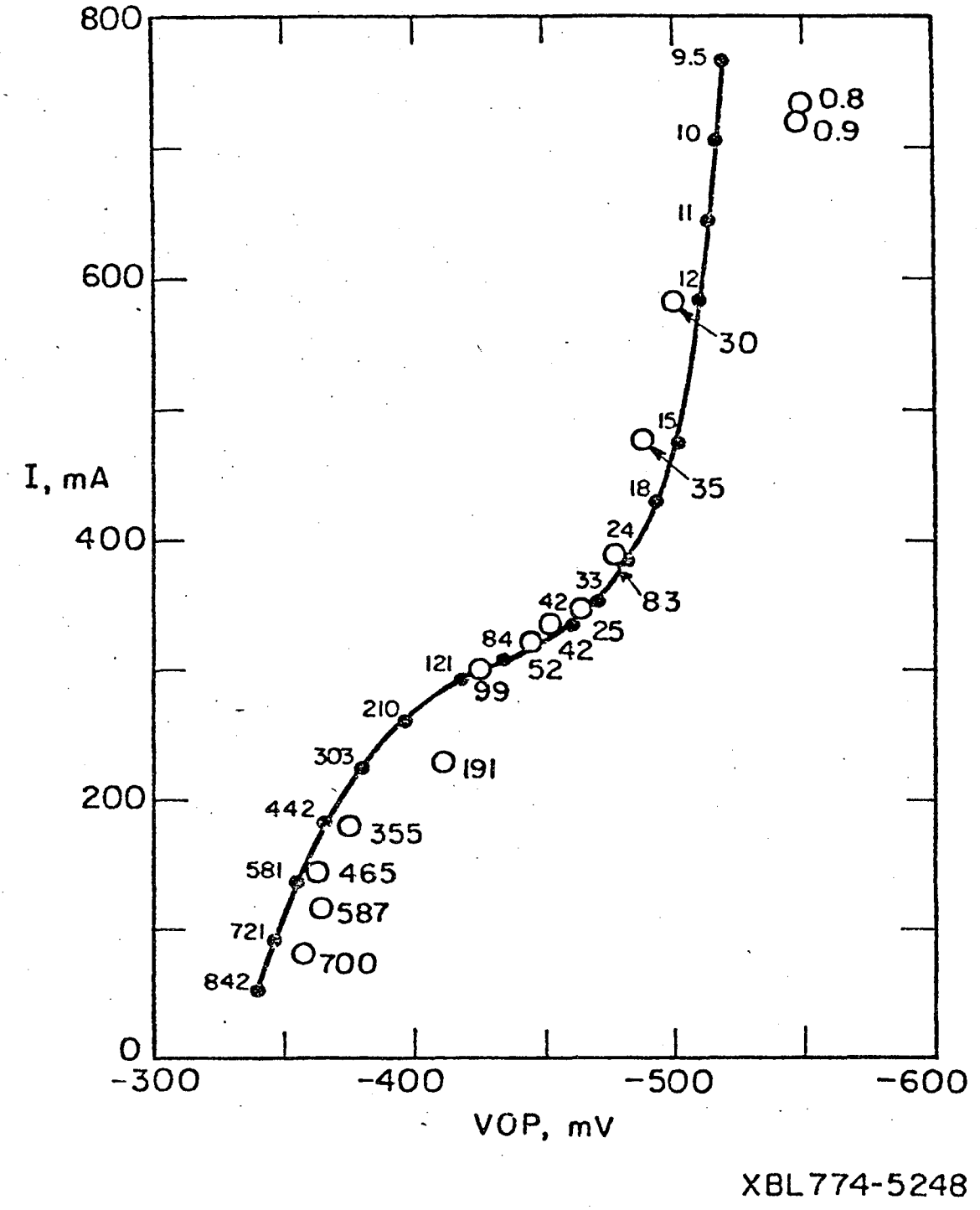

Figure 2. Current-potential curve for an electrode 5.5 cm deep and superficial electrode area of 61 cm^2, packed with carbon flakes and chips. Flowrate = 22 cm^3/min and the feed concentration = 1000 mg Ag/ℓ. Numbers below curve corresponding to the open circles 0 are experimental effluent concentrations (in mg/ℓ). The solid numbers above the curve correspond to the solid dots • are calculated effluent concentrations (in mg/ℓ). VOP in the potential of the current collector with respect to a saturated calomel reference electrode placed in the dilute product stream.

Table 3. Values of the parameters used in fitting the data in Figure 2 and in generating Figures 3 through 17.

Copper deposition with simultaneous generation of dissolved hydrogen

$a = 25cm^{-1}$ $\varepsilon = 0.3$ $D_o = 6\times10^{-6}cm^2/s$ $\kappa_o = 0.17mho/cm$ $s_R = -1$

$n = 2$ $T = 298.15\ K$ $\alpha_{aR} = 1.5$ $\alpha_{cR} = 0.5$ $\alpha_{aS} = 0.5$

$\alpha_{cS} = 0.5$ $U_S-U_R = 0.281\ V$ $L = 6cm$ $k_m = 0.1922\times10^{-3}cm/s$ $v = 3.328\times10^{-3}cm/s$

$i_{oR,ref} = 7.009\times10^{-6}A/cm^2$ $i_{oS,ref} = 3.717\times10^{-13}A/cm^2$ $c_{Rf} = 1.05\times10^{-5}mole/cm^3$

$c_{Sf} = 10^{-3}mole/cm^3$

Silver reduction with simultaneous reduction of thiosulfate

$a = 25cm^{-1}$ $\varepsilon = 0.3$ $D_o = 1\times10^{-5}cm/s$ $\kappa_o = 0.123mho/cm$ $s_R = -1$

$n = 1$ $T = 298.15\ K$ $\alpha_{aR} = 0.5$ $\alpha_{cR} = 0.5$ $\alpha_{aS} = 2.75$

$\alpha_{cS} = 1.25$ $U_S-U_R = 0.489\ V$ $L = 5.5cm$ $k_m = 3.330\times10^{-3}cm/s$ $v = 6.011\times10^{-3}cm/s$

$i_{oR,ref} = 9.134\times10^{-5}A/cm^2$ $i_{oS,ref} = 1.20\times10^{-22}A/cm^2$ $c_{Rf} = 9.27\times10^{-6}mole/cm^3$

$c_{Sf} = 0.951\times10^{-3}mole/cm^3$

Table 3. (continued)

Dimensionless parameters

	Copper	Silver
P_1	1.050×10^{-7}	9.404×10^{-4}
P_2	-3.254 to -6.508	-3.738 to -7.476
P_3	1.247×10^{-4}	5.364×10^{-4}
P_4	5.863×10^{-8}	6.341×10^{-46}
P_5	3.254	3.738
P_6	9.089×10^{-11} to 3.254	3.777×10^{-15} to 3.738
D'	0.1217	0.1168

$$S_2O_3^{2-} + 8e^- + 8H^+ \rightarrow 2HS^- + 3H_2O \ , \qquad [16]$$

where the standard electrode potential can be calculated[13,14] to be $U^{\theta}_{HS^-/S_2O_3^{2-}} = 0.221$ V ; one value each for the transfer coefficients for the side reaction α_{aS} and α_{cS} , which were assumed to sum to four. The freedom to assign arbitrary values to α_{aS} and α_{cS} is allowed in the model since the composition dependence of the polarization equation for the side reaction is neglected.

The value of the mass transfer coefficient k_m used in fitting the data was that obtained in fitting the data of Bennion and Newman,[11] which was correlated to be[1]

$$\frac{\varepsilon k_m}{aD_o} = 0.07054 \left(\frac{v}{aD_o}\right)^{0.5454} \ . \qquad [17]$$

In obtaining the fit to the silver removal data in Figure 2, it should not be interpreted that there is anything fundamental about the values of the fitted dimensional parameters found in Table 3, because not only are the data insufficient, but also the electrode is operating with a highly non-uniform current density and mass-transport limitations dominate in certain regions.

The model predictions of the current-potential behavior in Figure 2 are in satisfactory agreement with experimental data between 50 mA and 500 mA total current. However, at higher currents (above 500 mA), the data indicate the beginning of an additional limiting-current plateau, and agreement of the model calculations cannot be expected for

the following reasons: 1) the postulated side reaction[10] (equation 16) for the reduction of thiosulfate could be incorrect and there appears to be no fundamental kinetic information on this reaction and 2) if the limiting reactant species for the higher plateau were known, the model used here would not be sufficient since the concentration dependence for the side reaction was neglected and a more general model such as the one proposed by Alkire and Gould[4] would be more appropriate.

Agreement between model predictions for the silver effluent concentration and the experimental values shown in Figure 2, are satisfactory near the limiting current. This is because the model parameters were chosen so as to fit the data in this region. However, agreement should not be expected over the entire current-potential range because the data exhibit unexplained anomalies[10]: 1) current efficiencies above 100 percent and 2) a minimum in the silver effluent concentration with increasing values of VOP.

A comparison of the dimensionless parameters in Table 3 between the two chemical systems suggests that the parameters P_1 and P_3 account primarily for the difference in behavior of these systems. The parameters P_1 and P_3 represent the relative importance of the backward rate of the main reaction and the forward rate of the side reaction and are 10^4 and 4.3 times greater, respectively, for the silver system than for the copper system. As will be observed later a low effluent concentration cannot be achieved for silver system and this is due to the combined effect of the parameters P_1 and P_3.

The magnitude of the side reaction is substantial for the silver system and this shields the back of the electrode (in the case of an upstream counterelectrode) from having a large electric driving force which results in a very small rate for the deposition of silver in this region. This is accentuated by the fact that P_1 is large, which causes the backward rate of the deposition reaction to be of the same order on the forward rate and the reactor can become thermodynamically limited.

Results and Discussion

As a unifying concept here, let us consider how we can achieve a very high conversion or, equivalently, a very low effluent concentration of the limiting reactant while, at the same time, operating the reactor at as high a flow rate as possible. Towards these ends, we can consider variations of electrode current density and length, flow rate, configuration, and matrix conductivity. By means of the computer program, we have the means to investigate in detail how the presence of a side reaction places limitations on the attainment of these goals.

Effect of electrode length. For the case of a very high matrix conductivity, Figure 3 shows the effect of electrode length and current density on the effluent concentration for the copper system. We see, first of all, that we must operate at or above the limiting current in order to reach a really low effluent concentration. If we operate at $I^* = 0.9501$, we cannot expect to remove more than 95 percent

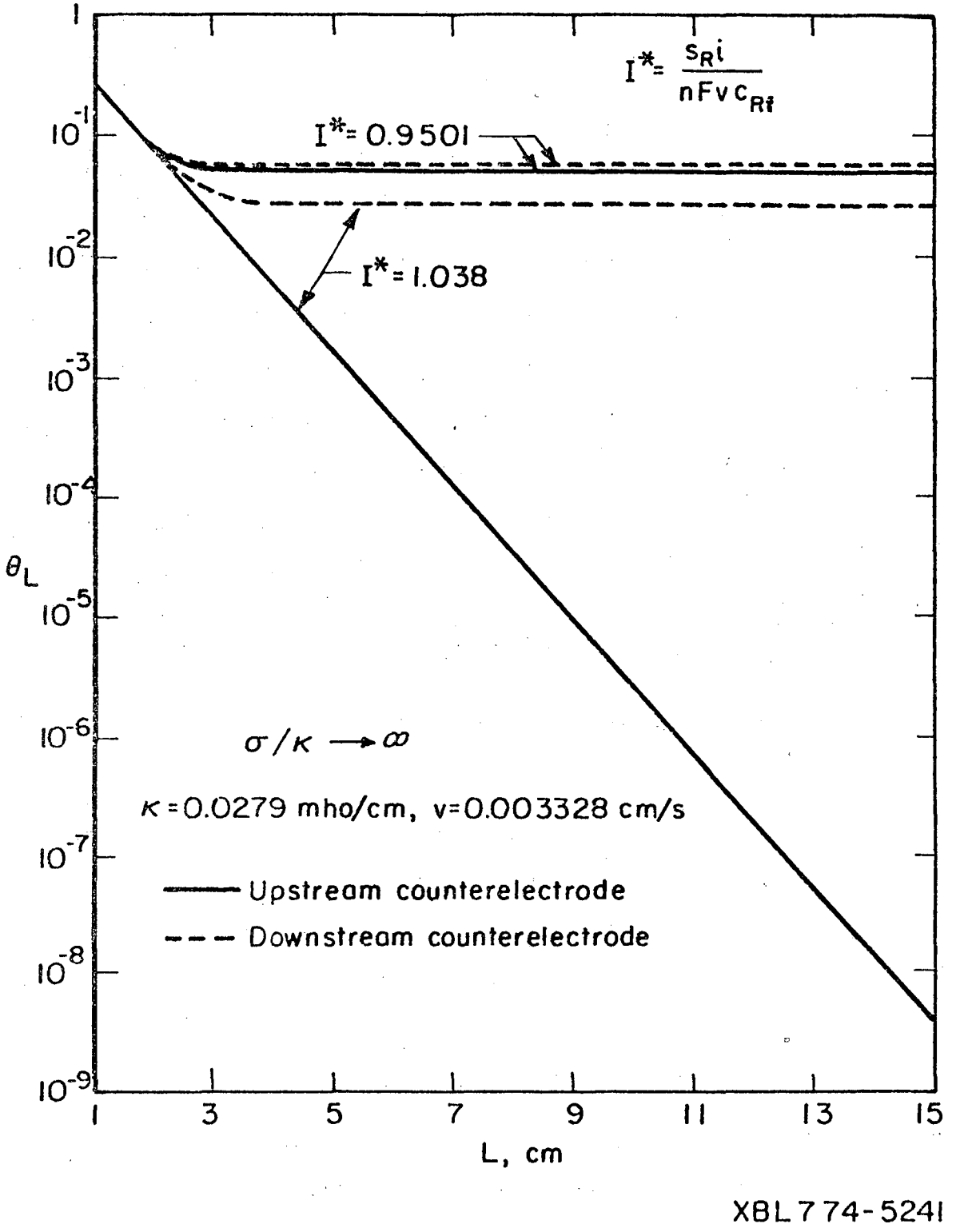

Figure 3. Effluent copper concentration as a function of electrode length for $c_{Rf} = 0.0105$ M .

of the copper even if we have very high current efficiencies and substantial electrode lengths.

The curve on Figure 3 for an upstream counterelectrode and $I^* = 1.038$ shows essentially a limiting-current condition -- the effluent concentration decreases almost exponentially with electrode length. (See, for example, the analysis of Bennion and Newman[11] and that of Newman and Tiedemann[15] when axial diffusion and dispersion are included.) However, for downstream placement of the counterelectrode, a limiting-current distribution cannot be maintained except for electrode lengths less than 2 cm, and a truly low effluent concentration cannot be attained at all with this electrode configuration (at this flow rate). The current efficiency must necessarily be somewhat lower, and the extent of the side reaction somewhat higher, with the downstream counterelectrode.

Figures 4 and 5 introduce the effect of a finite matrix conductivity σ. Now, according to Figure 1, four different configurations are relevant since the placement of the current collector must also be considered. Figure 4 shows that the UU configuration retains the exponential decrease of θ_L with L, although performance is slightly degraded by the additional ohmic potential drop compared to the case of the infinite matrix conductivity. (The curve for $\sigma = 10\,\kappa$ will be discussed later in connection with the optimum matrix conductivity.) Figure 5 shows the relatively poor performance achievable with the other configurations. In these cases, the ohmic potential drop in the matrix and solution phases prevents the entire reactor from being

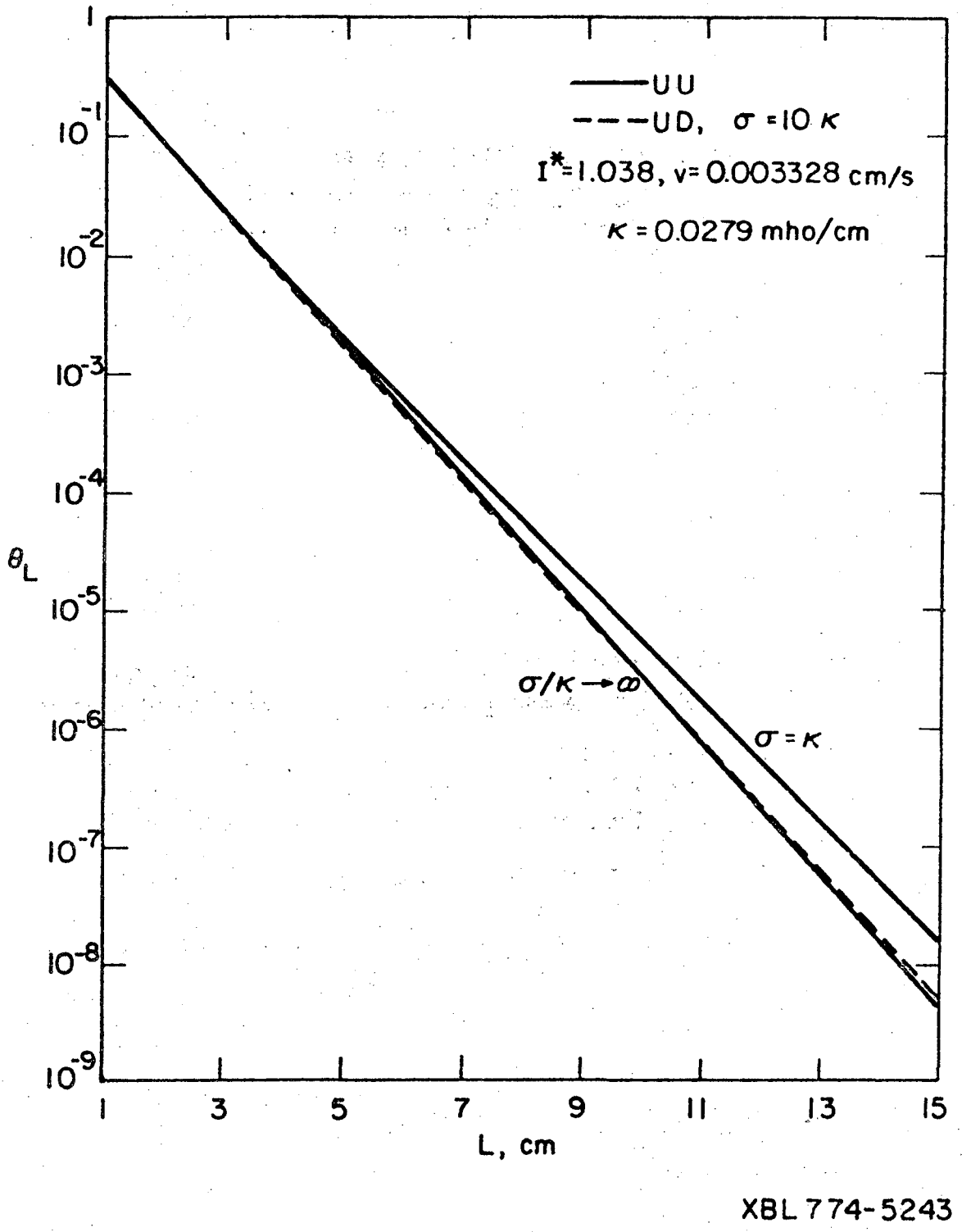

Figure 4. Effluent copper concentration as a function of electrode length.

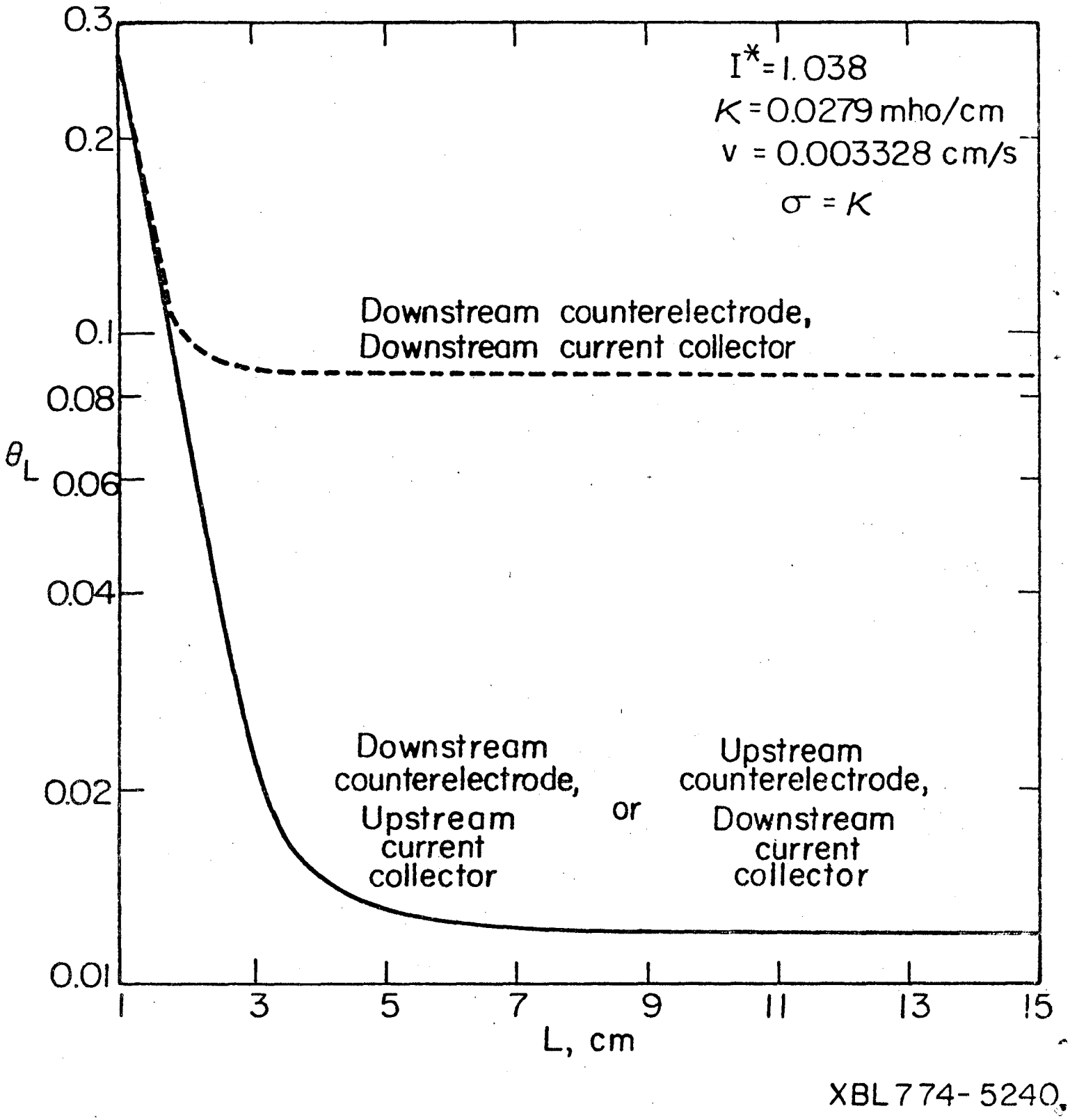

Figure 5. Effluent copper concentration as a function of electrode length.

operated at a limiting-current condition, as we shall discuss in more detail later.

Figure 6 displays the silver effluent concentration as a function of electrode length for the various electrode configurations for cases where $\sigma >> \kappa$ and $\sigma = \kappa$. The results show that none of the electrode configurations yields an exponential decrease in θ_L with electrode length; thus a limiting-current distribution cannot be achieved in any of the geometries due to extensive interference by the side reaction.

Effect of matrix conductivity. Figures 7 and 8 show the dependence of the effluent copper concentration on the matrix resistivity $(1/\sigma)$. Figure 9 shows similar results for the silver system. Calculations for a DD placement are not presented here since this configuration does not allow a low effluent concentration, in comparison to the other configurations when the matrix conductivity is small.

In Figures 7 and 9, we observe that the UD configuration exhibits a minimum with matrix resistivity and therefore has an optimum value for σ (about equal to 0.1 κ for the copper system). On the other hand, for the UU configuration, θ_L increases monotonically with increasing matrix resistivity. The DU configuration on Figure 8 would also show a minimum at values of κ/σ substantially greater than unity. This is of less interest than the minima for the UD configuration because matrix resistivities are usually much less than solution-phase resistivities and because the effluent concentrations are inherently large with the DU configuration. For example, the DU and UD configurations

Figure 6. Effluent silver concentration as a function of electrode length for c_{Rf} = 0.00927 M .

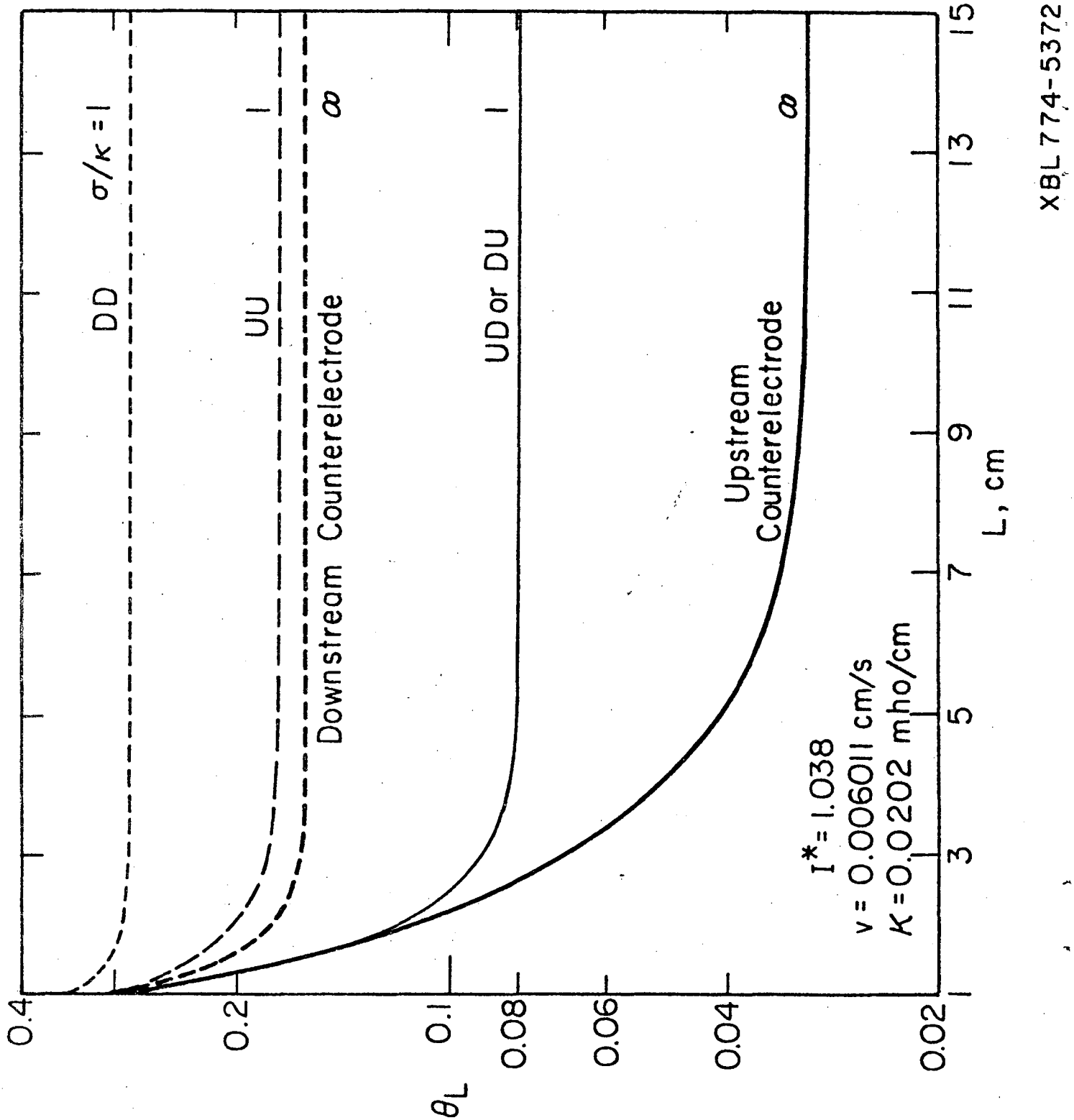

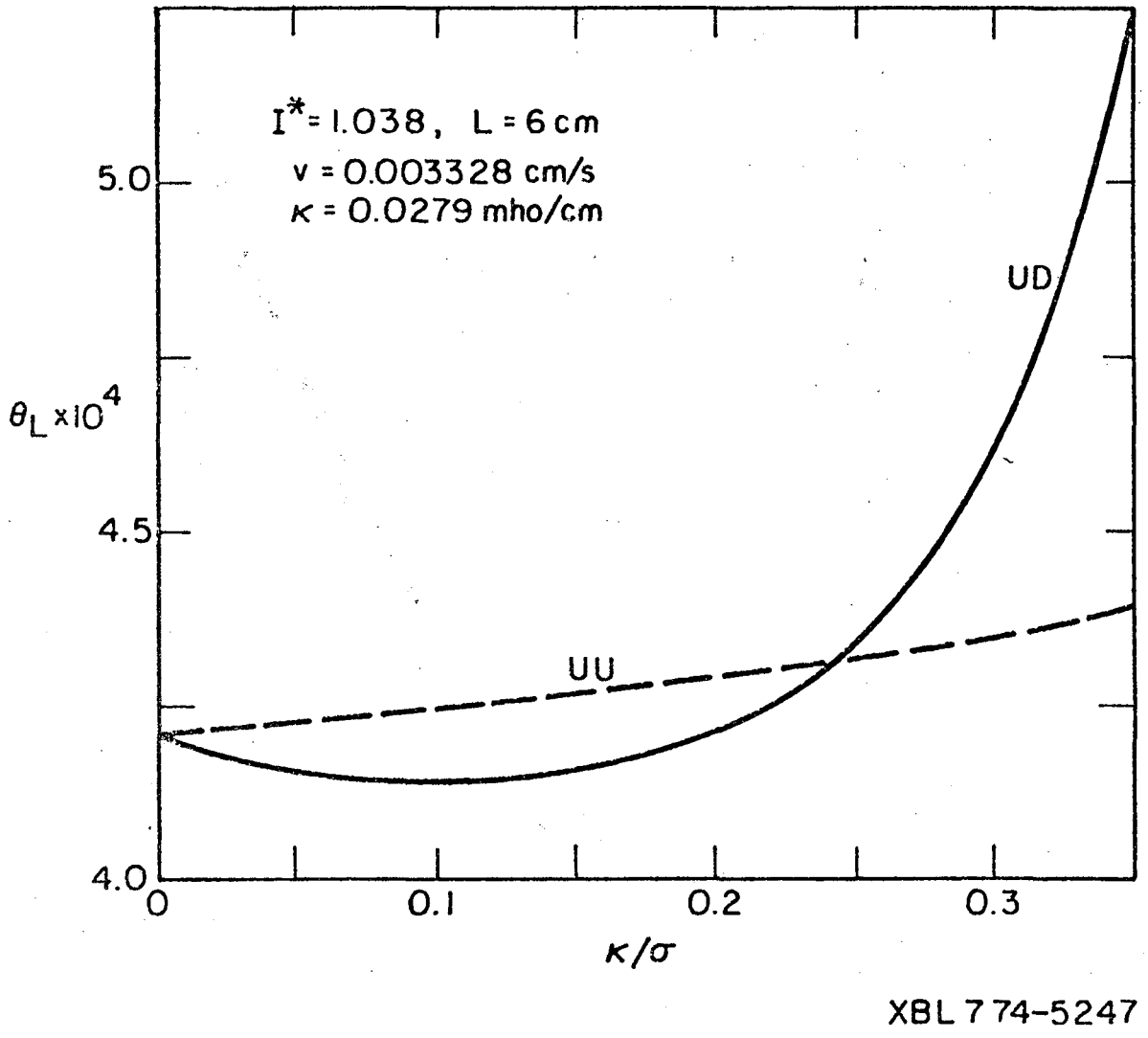

Figure 7. Dependence of the copper effluent concentration on the matrix resistivity.

Figure 8. Dependence of the copper effluent concentration on the matrix resistivity.

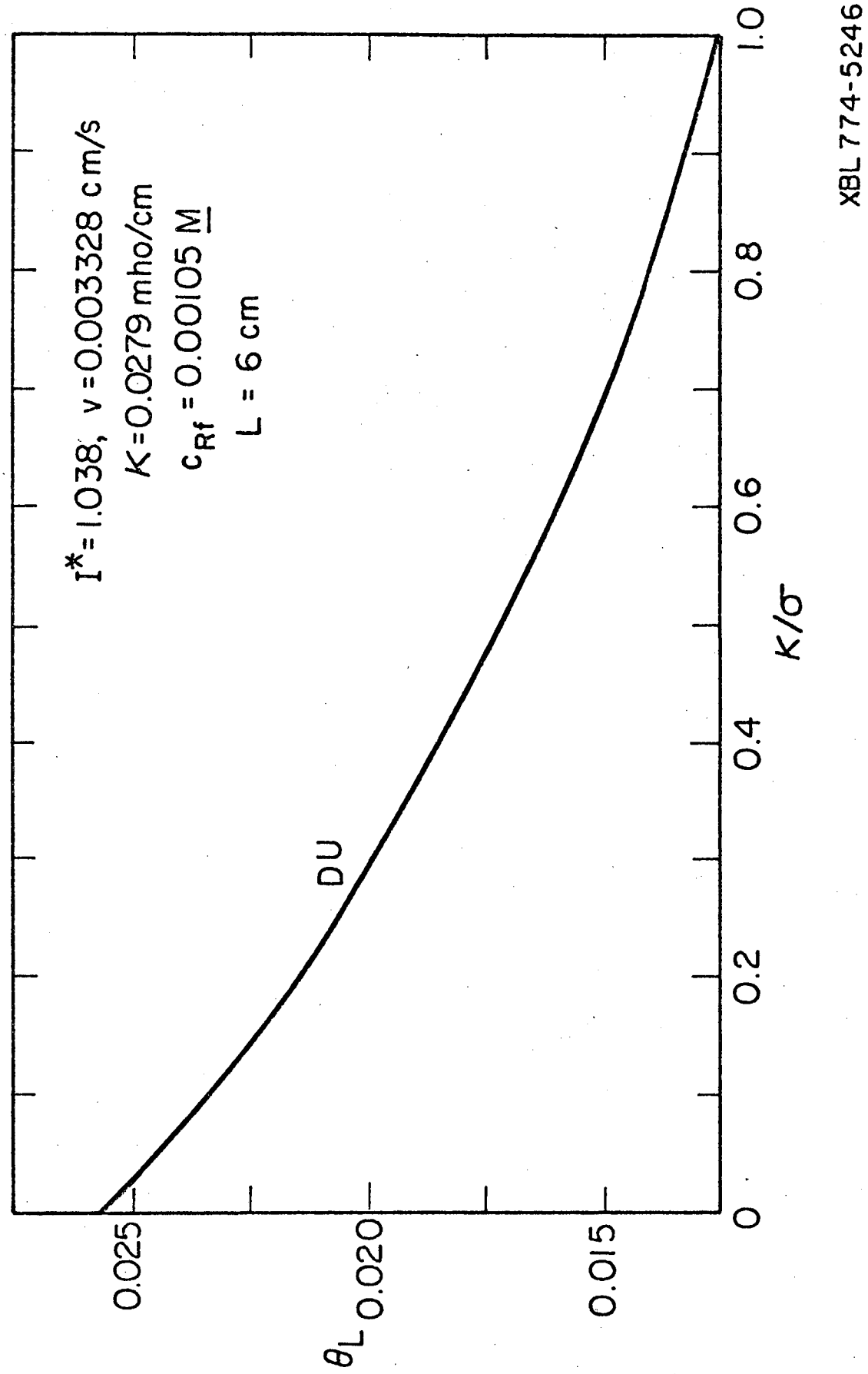

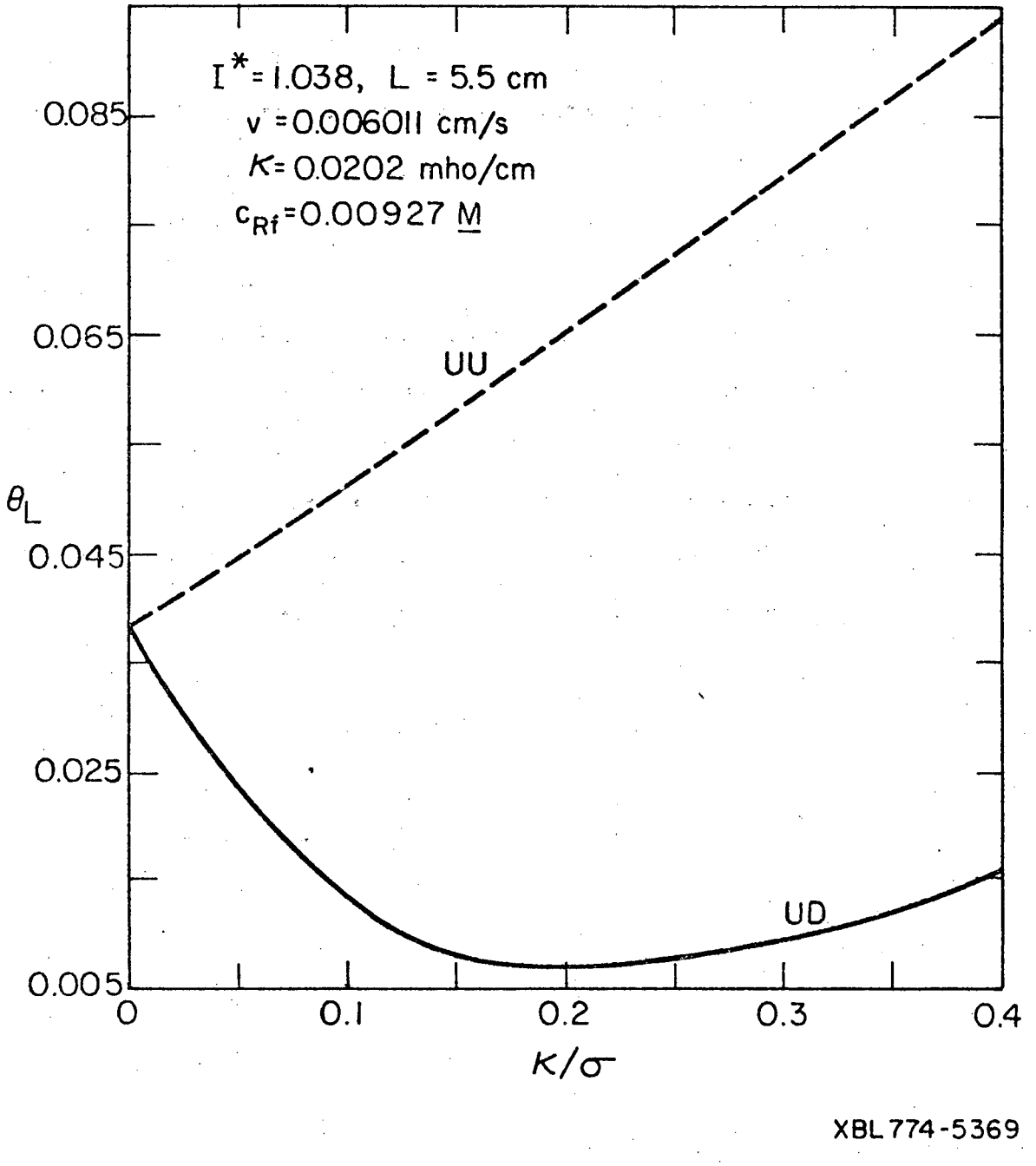

Figure 9. Dependence of the silver effluent concentration on the matrix resistivity.

give the same effluent concentration when $\sigma = \kappa$ (see Figure 5) but at this point, the value of θ_L has risen to 0.0125 from a minimum of 4.14×10^{-4} on Figure 7. At $\sigma = \kappa$, the UU configuration is still able to attain a value of θ_L of 6.08×10^{-4} (see Figure 4). [Note, however, that the DU configuration performs better than the UU configuration for $\sigma = \kappa$ in the silver system, as displayed on Figure 6.]

Return for a moment to the dashed curve on Figure 4. For this curve, $\sigma = 10\ \kappa$, which corresponds to the minimum for the UD configuration shown in Figure 7, and an exponential dependence of θ_L on L can evidently be maintained. The performance is superior to the high-matrix-conductivity case for L less than about 10 cm, after which it becomes somewhat inferior. The optimum ratio of κ/σ depends on electrode length, for example, for an electrode 4 cm in length the optimum ratio is approximately 0.17, for an electrode 8 cm long the optimum ratio is approximately 0.07. Note that we get a markedly different view of the effect of configuration and matrix resistivity if we confine our attention to the cases $\sigma >> \kappa$ and $\sigma = \kappa$ on Figures 3, 4, and 5 from what we get if we include the variation of σ and the optimum value of σ. The UD configuration is totally unsatisfactory at $\sigma = \kappa$ but excellent at $\sigma = 10\ \kappa$.

For the silver system, other calculations show that, even at the optimum ratio of $\kappa/\sigma = 0.2$ shown on Figure 9 for the UD configuration, a limiting-current distribution and an exponential dependence of θ_L on L cannot be achieved. Similar results for the copper system can be obtained by increasing the flow rate to somewhat less than three times the value used in calculating Figures 3, 4, and 5.

Bennion and Newman[11] have formulated design considerations for achieving a low effluent concentration while operating at as high a flow rate as possible. First, the electric driving force within the electrode must be maintained high enough to attain a limiting-current condition throughout the reactor. The electric driving force must also be maintained low enough to avoid excessive side reactions. These two conditions thus define a limited range of potentials allowable within the reactor. Since the electrode must be of substantial length in order to achieve a given effluent concentration, there is an upper limit on the flow rate above which these constraints cannot be satisfied simultaneously.

The effect of the side reaction is not one which can be compensated for by using a longer electrode or a higher current, even if one is willing to pay the price of a lower current efficiency and a higher cell potential. It is a characteristic of porous electrodes, leading to their inherently nonuniform reaction rate distributions, that substantial current densities flowing over substantial distances in either the matrix or solution phases make it impossible to maintain a uniform electric driving force (for the reactions) throughout the electrode.

On the basis of these considerations, an important quantity is the difference between the minimum electric driving force η_{min} and the maximum electric driving force η_{max} that prevail within the reactor. Figure 10 displays this quantity as a function of the conductivity ratio for the copper system and corresponds directly with the

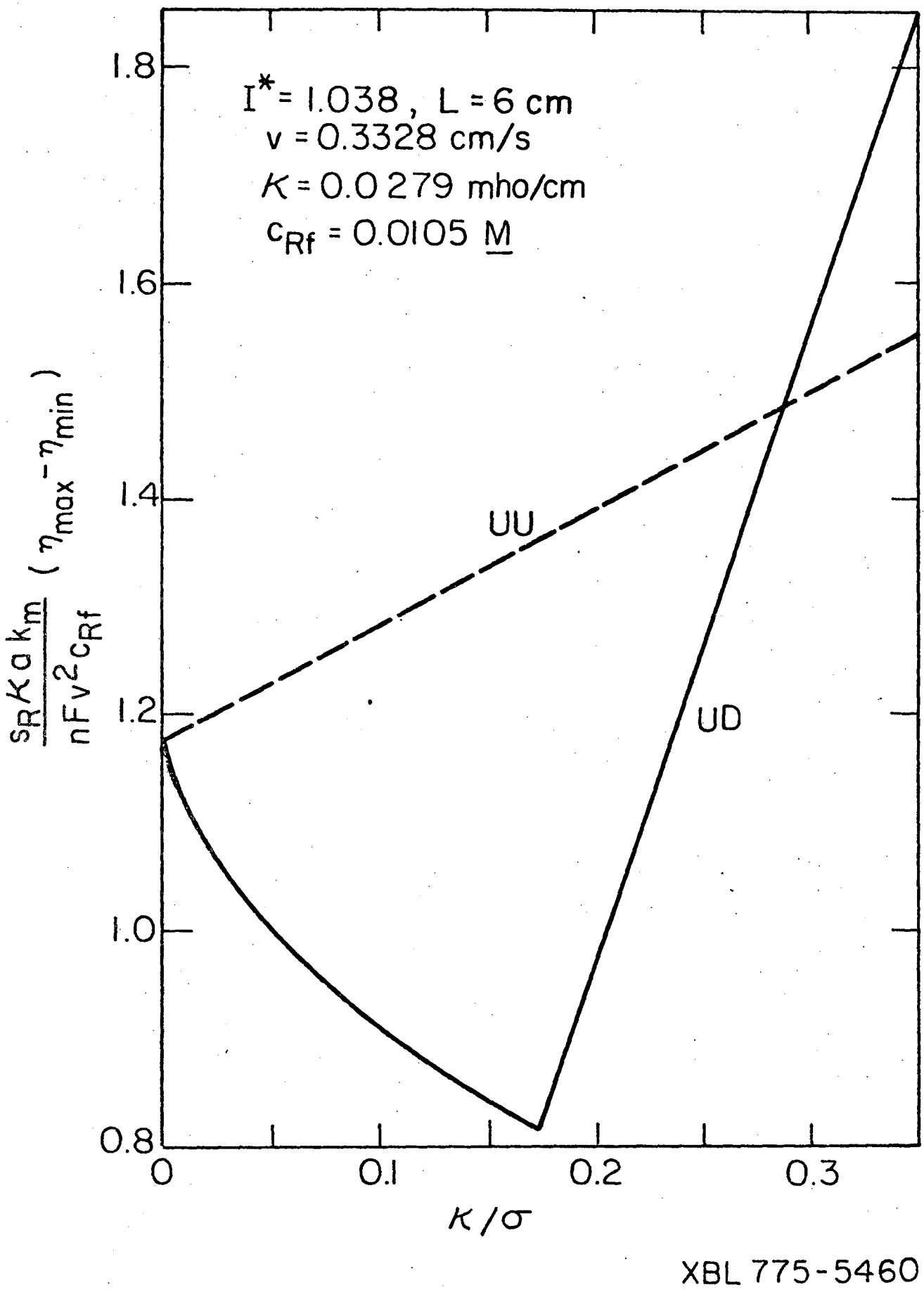

Figure 10. Variation in the difference between the maximum and minimum driving force for copper deposition with the matrix resistivity.

conditions of Figure 7. The ordinate, made dimensionless with $nFv^2c_{Rf}/s_R\kappa ak_m$, will have a magnitude on the order of unity if the current density is distributed like that for the limiting current for the main reaction.[11,15] A graph similar to Figure 10 is given by Newman and Tiedemann[15] for the case where the current densities are calculated according to the limiting-current distribution for the main reaction. The computer program used here permits analysis above and below the limiting current and in the presence of a side reaction.

The fact that the ordinate values on Figure 10 are of order unity illustrates how the constraints on the flow-through porous electrode can better be satisfied by operation at lower flow rates.

There is a correspondence between the shapes of the curves on Figures 7 and 10. Conditions which lead to an inherently smaller value of $|\eta_{max} - \eta_{min}|$ make it possible to achieve a limiting-current condition through a larger portion of the reactor, without extensive side reaction. For the UD configuration, the maximum electric driving force occurs at the fluid inlet for $\kappa/\sigma < 0.175$. The position of the maximum electric driving force then shifts to the fluid outlet for $\kappa/\sigma > 0.175$. This leads to the sharp minimum for the UD configuration in Figure 10.

Detailed distributions. The behavior of these systems can be understood better by consideration of the calculated current, potential, and electric-driving-force distributions within the electrode. These are illustrated for the copper system with an electrode 6 cm long and by a 5.5 cm electrode for the silver system.

For the copper system with an infinite matrix conductivity, Figure 11 shows the relative rates of reaction for both the main and side reactions for both upstream and downstream placement of the counterelectrode. Figure 12 shows the corresponding distributions of potential in the matrix and pore solution. The total current density to the electrode was chosen close to the limiting current ($I^* = 1.038$) for the deposition of copper. For upstream placement of the counter-electrode, the main reaction rate decreases almost exponentially with distance through the electrode (as predicted by the limiting-current analyses in references 11 and 15). At the same time, the side reaction follows the electric driving force (see Figure 12), which is high at the fluid inlet and decreases toward a uniform value near the fluid outlet.

On the other hand, for the downstream placement of the counter-electrode, the main reaction rate does not show an exponential dependence on distance. Figure 12 shows that the electric driving force is very large at the outlet but too low at the inlet. Consequently, a limiting-current condition is not maintained near the front. At about 65 percent of the distance through the electrode, the electric driving force has become large enough to assure a limiting-current condition, and subsequently an exponential dependence on distance is exhibited. However, failure to utilize effectively the front part of the electrode makes it impossible to achieve a truly low effluent concentration, and increasing the electrode length would not help (see Figure 3). The resulting reaction-rate distribution now has a maximum; as the electric driving force increases toward the back of the electrode, the reaction rate goes up,

Figure 10. Current distributions for deposition of copper and generation of dissolved hydrogen within a porous electrode. Calculated for c_{Rf} = 0.0105 M .

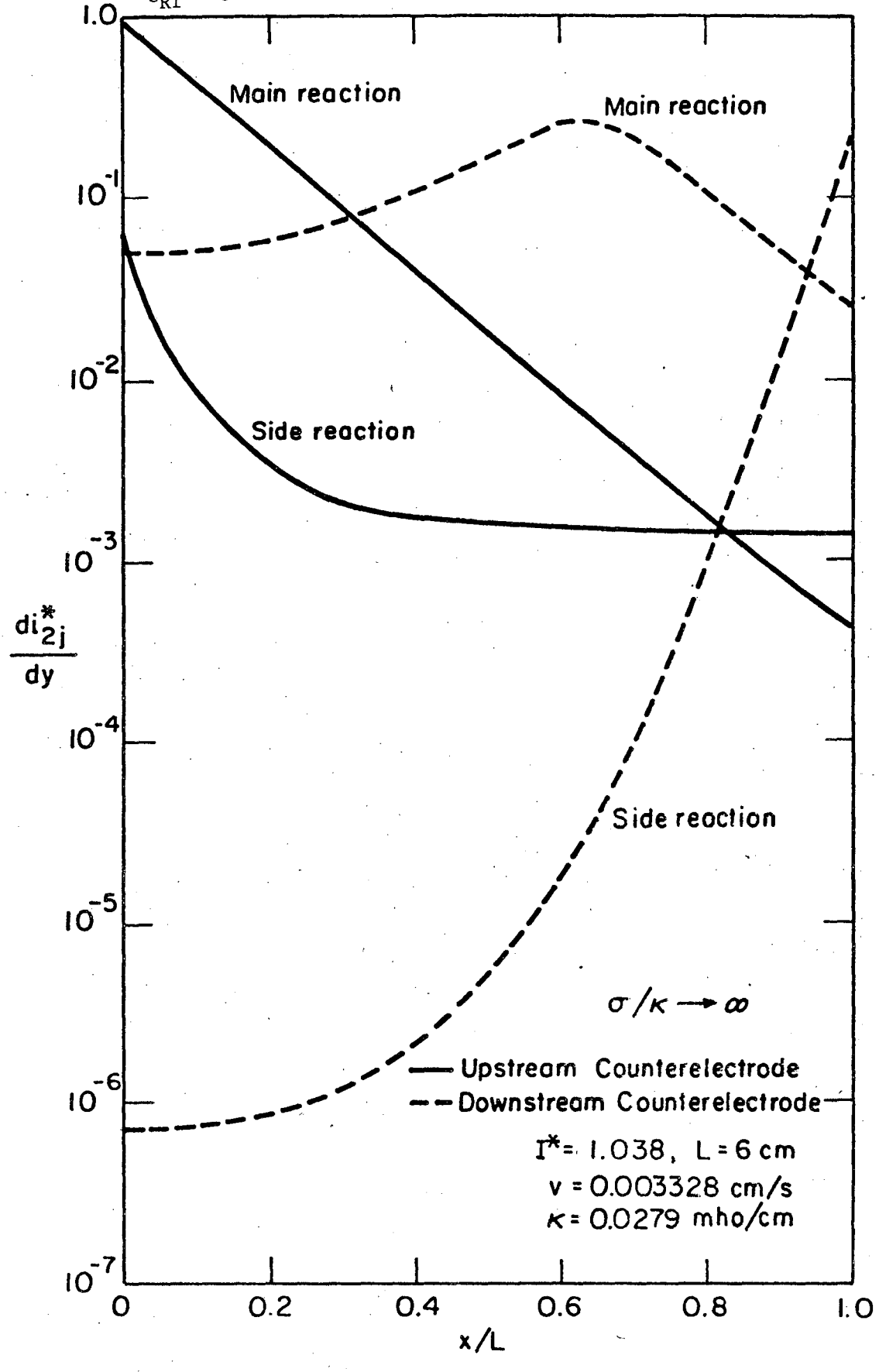

XBL774-5244

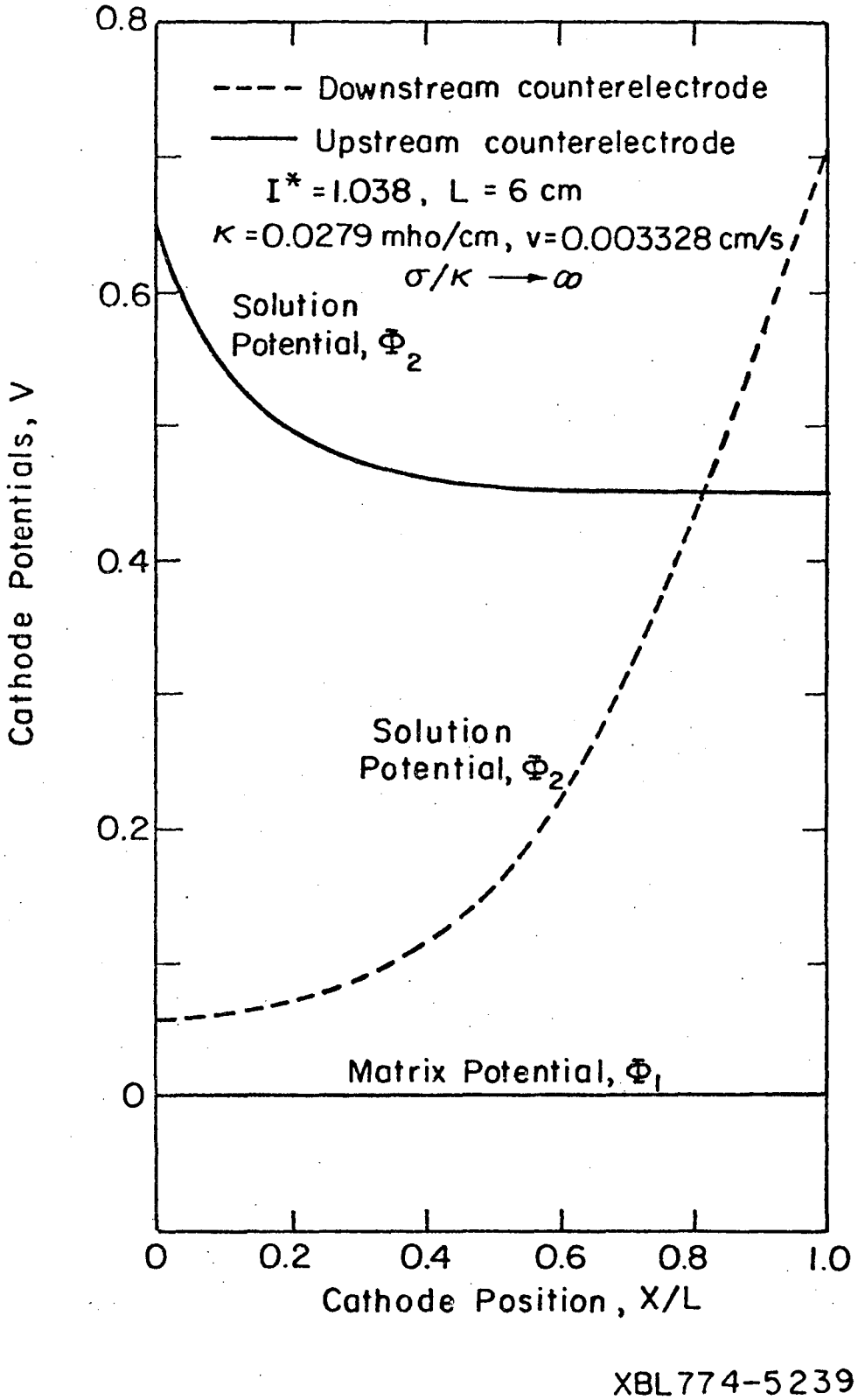

Figure 12. Calculated solution phase and solid matrix phase potential distributions for the deposition of copper and simultaneous formation of dissolved hydrogen.

and copper is depleted from the solution to the extent that the mass-transfer driving force becomes small. The reaction rate exhibits a maximum and then decreases with distance. (Similar reaction-rate distributions have been reported by Alkire and Gould.[4] These are examples of a general phenomenon[16-19] resulting from the competition of electric and mass-transfer driving forces.) The side reaction has a distribution in Figure 11 that again follows that of the electric driving force in Figure 12. Because of the somewhat lower rate of the main reaction, in comparison to the upstream placement of the counter-electrode, the side reaction now occurs at a somewhat higher rate on the average. For these comparisons at a constant total current ($I^* = 1.038$), an increase in the effluent concentration from one electrode to another is accompanied by a corresponding decrease in the current efficiency.

As in porous electrodes in general, the reaction rate distributions and ohmic potential drop shield the more remote parts of the reactor from having an adequate electric driving force. In this particular situation, the contrast between the cases of upstream and downstream placement of the counterelectrode arises in the following way. In order for there to be a high conversion, there must be a high reaction rate -- generating high current densities in the solution -- near the fluid inlet. Since the solution-phase conductivity κ is not high, potential variations in the solution phase can be minimized if the current flows out of the electrode at the nearest possible point, namely, to a counterelectrode placed upstream. If the counterelectrode

is placed downstream, the large currents which should be generated near the fluid inlet must flow in the solution through most of the thickness of the electrode, and this necessarily leads to large variations of potential. A similar explanation applies in the more complex cases to follow, where the matrix conductivity is also finite.

Figure 13 shows the reaction-rate distributions for the main and side reactions for the copper system where $\sigma = \kappa$. The corresponding potential distributions are shown in Figure 14. Because of the complexity of Figure 14, the distributions of electric driving force are also shown in Figure 15.

The reaction-rate and electric-driving-force distributions for the UD and DU configurations happen to be identical when $\sigma = \kappa$ since the boundary conditions given in Table 3 are then identical. However, the potential distributions in each phase will be different, as seen in Figure 14. In these configurations, the counterelectrode and the current collector are not at the same end of the reactor. Consequently, the current flows in the same direction in the matrix as in the solution, and to a certain extent the potential drop in the matrix can match that in the solution (see Figure 14). This makes it possible, in some cases, to reduce the variation of the electric-driving-force within the reactor (see Figure 10). It also means that the extreme values of the electric driving force occur at the ends of the reactor, with the minimum value occurring somewhere between (see Figure 15), and the side reaction follows this distribution (see Figure 13).

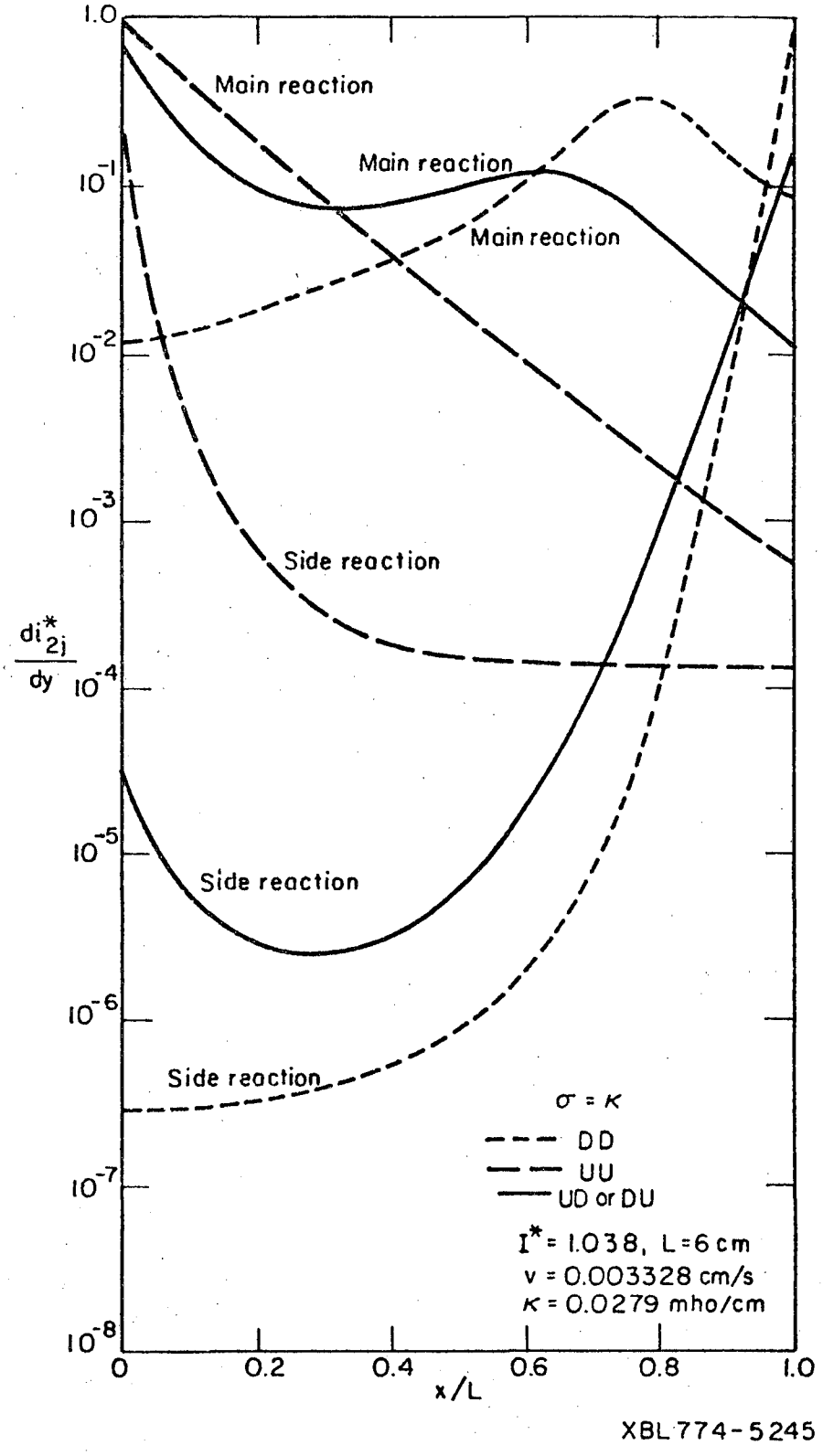

Figure 13. Current distributions for deposition of copper and generation of dissolved hydrogen within a porous electrode. Calculated for c_{Rf} = 0.0105 M .

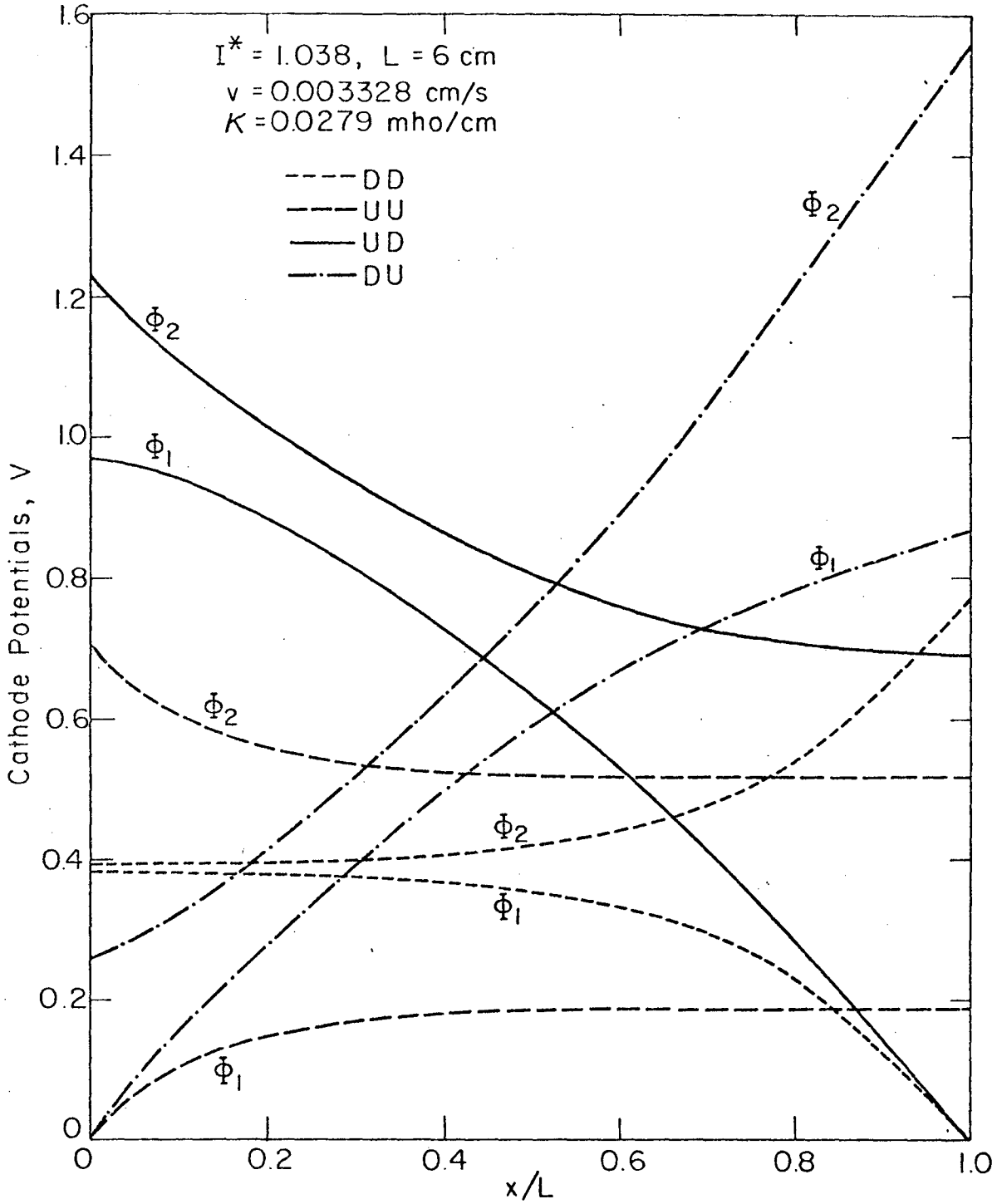

XBL774-5374

Figure 14. Calculated solution phase and solid matrix phase potential distributions when $\sigma = \kappa$ for the depositions of copper and simultaneous formation of dissolved hydrogen.

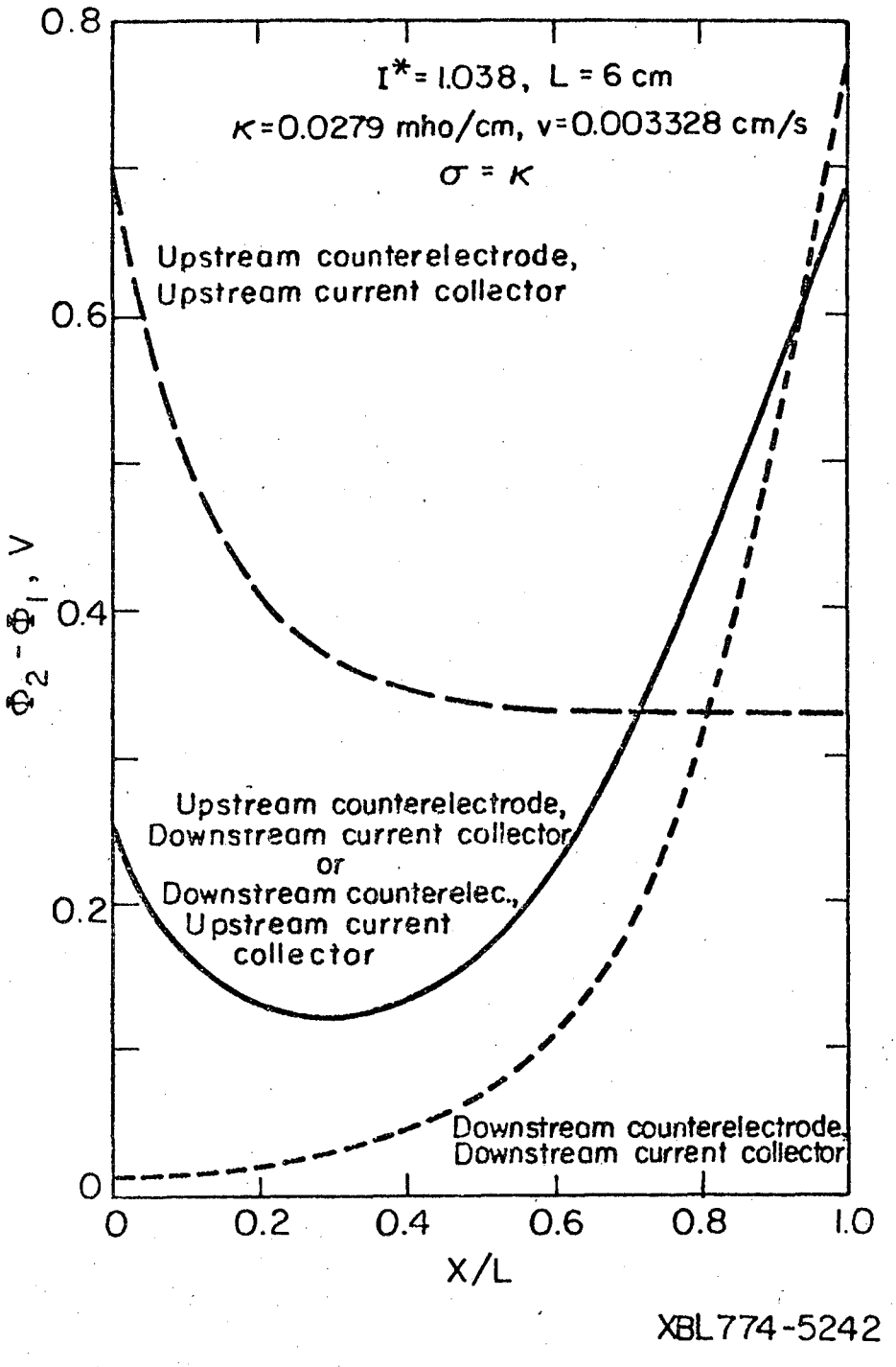

Figure 15. Electrical driving force distributions for the potential distributions shown in Figure 14.

For the UU configuration, the maximum electric driving force occurs at the inlet, and the minimum at the outlet, and conversely for the DD configuration. For the main reaction, only the UU configuration shows an exponential dependence of rate on distance (see Figure 13). For the other configurations, the main reaction is below the limiting current for a substantial (DD) or moderate (UD or DU) region near the inlet, and consequently the effluent concentration cannot be reduced to a truly low value. Only in the UU configuration are the current densities in both the solution and matrix phases small near the back of the electrode. In this region the electric driving force varies little (as is the case also for the upstream counterelectrode case in Figure 12, where $\sigma >> \kappa$), and measurement of $\Phi_1 - \Phi_2$ at $x = L$ can lead to a lower-bound thermodynamic estimate of the minimum attainable concentration in a flow-through porous electrode.[12]

Figures 16 and 17 show the reaction-rate and electric-driving-force distributions for the silver system. A limiting-current distribution is not achieved for any electrode configuration, due to extensive interference by the side reaction, as indeed, it is not, even for an infinite matrix conductivity (see Figure 6). As for the copper system, the electric driving force for the DD configuration is small at the front of the electrode, and for the UD and DU configurations it is small in the middle and only moderately large at the front. Under these conditions, the front and middle regions of the reactor are not effectively utilized, and a low effluent concentration cannot be achieved even though a limiting-current condition is maintained near the rear.

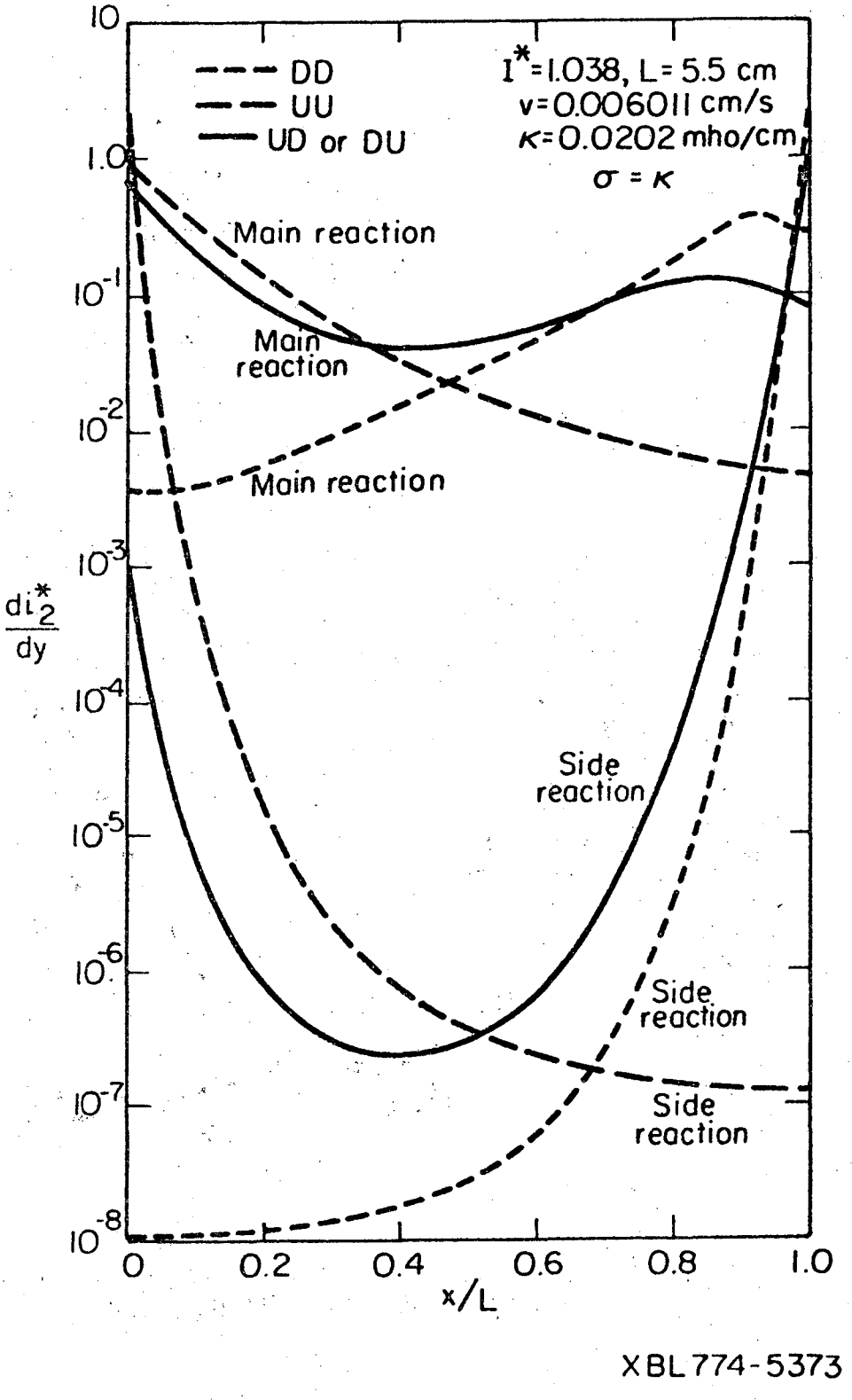

Figure 16. Current distributions for silver deposition and reduction of thiosulfate within a porous electrode. Calculated for c_{Rf} = 0.00927 M , and L = 5.5 cm .

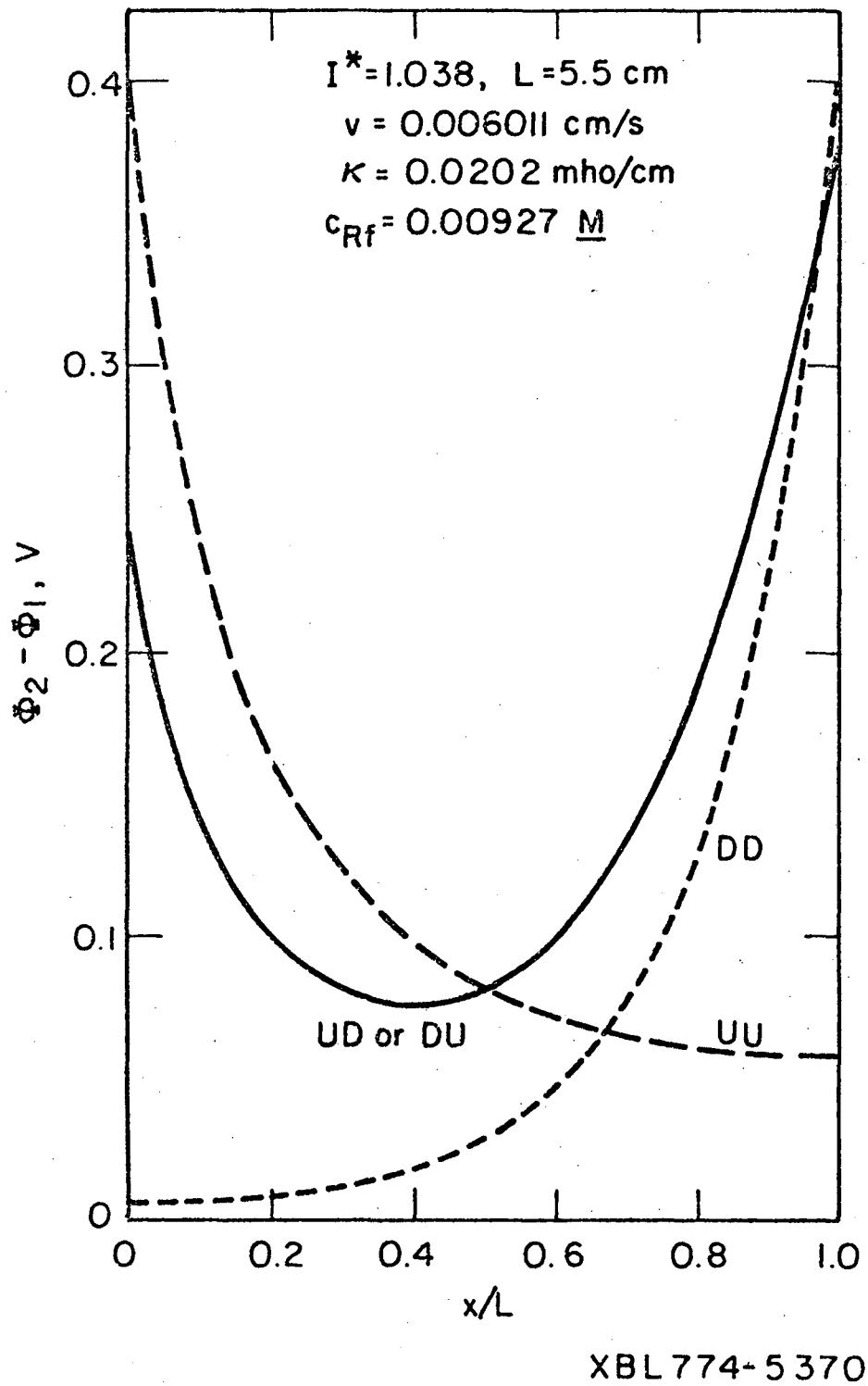

Figure 17. Electrical driving force distributions for the deposition of silver from thiosulfate solutions.

However, for the UU configuration, the lowest electric driving force occurs at the rear of the reactor, and the rate of the main reaction does not decrease exponentially with distance. In fact, with the higher value of P_1 for the silver system, the effluent concentration is very close to the thermodynamic limit determined by the electric driving force prevailing at the fluid outlet.[12]

Effect of configuration. The preceding discussion has permitted a comparison of several configurations under a variety of operating conditions. It is important to recognize that the lowest effluent concentration is achieved for upstream placement of the counterelectrode (see Figures 3 through 6). For downstream placement of the counter-electrode, a limiting-current distribution cannot be obtained (see Figures 11 and 13), principally because the current in the solution must flow through most of the length of the electrode, and this leads to a large ohmic potential drop.

For the DU configuration shown in Figure 8, θ_L decreases with increasing values of matrix resistivity. For a downstream counter-electrode, a situation is created where the ohmic potential drop in the solution is working against the favorable mass-transfer condition near the fluid inlet. Increasing the matrix resistivity increases the electric driving force near the fluid inlet because the matrix current must leave through the current collector placed there. This causes the rate of the main reaction at the front of the electrode to increase from about 0.05 when $1/\sigma \to 0$ (in Figure 11) to 0.67 when $\sigma = \kappa$ (in Figure 13).

As mentioned earlier, the DD configuration is the least efficient of the configurations shown in Figure 1. If the matrix resistivity is increased from zero, the electric driving force is further reduced near the fluid inlet, while it increases somewhat near the fluid outlet (compare Figures 14 and 15 with Figure 12). This causes the rate of the main reaction near the front to decrease from about 0.05 when $1/\sigma \to 0$ to 0.012 when $\sigma = \kappa$ (see Figures 11 and 13). Since the rear of the electrode was already at a limiting current, the increase in the electric driving force in this region is of little benefit; the rate of the main reaction is higher than with $1/\sigma \to 0$ because the flowing stream was not depleted as much in the upstream region, not because the electric driving force is larger. The integrated reaction rate is 6.3 percent lower when $\sigma = \kappa$, and the rest of the current goes into the side reaction, driven by the higher electric driving force near the rear.

For upstream placement of the counterelectrode, conditions are already more favorable when the matrix resistivity is small. For the UU configuration, increase of $1/\sigma$ decreases the electric driving force in the rear region and causes the current locally to drop below the limiting value. Consequently, θ_L increases, as shown in Figure 7 and 9. For the UD configuration, the electric driving force decreases near the inlet and increases near the outlet as $1/\sigma$ increases. This is favorable until the reaction rate drops below the limiting value near the inlet, and this leads to the minimum in the curve of θ_L versus κ/σ. The choice between the UD and UU configurations is

dependent on the chemical system and the matrix conductivity. However, the UD configuration will display a minimum in the effluent concentration as a function of κ/σ and is therefore the best configuration if this electrode could be built in practice.

Conclusions and Summary

A theoretical model for flow-through porous electrodes[1] has been used to evaluate the effects of electrode placement relative to the fluid inlet and finite matrix conductivity on the performance of flow-through porous electrodes. If a low effluent concentration is desired, the electrode must be operated at a superficial current density sufficiently high so that the main reaction may achieve a limiting-current distribution. Calculations show that a limiting-current distribution can only be achieved for upstream placement of the counterelectrode and not for a downstream counterelectrode. However, if interference by the side reaction is substantial, as is the case for silver removal from thiosulfate solutions or for the copper system if the superficial velocity is too high, a limiting-current distribution cannot be achieved for any electrode configuration at any matrix conductivity.

For an upstream counterelectrode when the matrix conductivity is not large, the choice between upstream or downstream placement of the current collector depends on the chemical system and what matrix conductivity can be achieved in practice.

Below the limiting current, the performance is only slightly better for an upstream counterelectrode than for downstream placement of the counterelectrode.

Calculations for a small matrix conductivity show that the DD configuration should probably never be built.

It is evident from the results that simple limiting-current calculations are inadequate for describing the behavior of flow-through porous electrodes. Thus, the ability to calculate distributions of current, potential, and concentration in the presence of side reaction above and below the limiting current makes it possible to choose the optimum electrode configuration so as to design and optimize an electrode system for the most economical removal of metal-ions.

Acknowledgment

This work was supported by the U.S. Energy Research and Development Administration.

Notation

a	specific interfacial area, cm^{-1}
c_{Rf}	upstream feed concentration of metal-ion reactant, $mole/cm^3$
DD	downstream counterelectrode, downstream current collector
DU	downstream counterelectrode, upstream current collector
c_S	hydrogen ion or thiosulfate ion concentration, $mole/cm^3$
D_a	axial dispersion coefficient of metal-ion reactant, cm^2/s
D_o	molecular diffusion coefficient of metal-ion reactant, cm^2/s
D_R	effective diffusion coefficient of metal ion reactant, cm^2/s
D'	dimensionless parameter describing the relative importance of axial diffusion and dispersion, see equation 32
F	Faraday's constant, 96487 C/equiv
i	superficial current density to an electrode, A/cm^2
$i_{oj,ref}$	exchange current density for reaction j at a reference composition $c_{i,ref}$, A/cm^2
i_1	superficial current density in the matrix, A/cm^2
i_2	superficial current density in pore-solution phase, A/cm^2
I^*	dimensionless superficial current density to an electrode, see equation 10
i_2^*	$= \frac{s_R i_2}{nFvc_{Rf}}$ dimensionless current density in pore-solution phase
I	total current to an electrode, A

k_m average mass-transfer coefficient between flowing solution and electrode surface, cm/s

L thickness of porous electrode, cm

n number of electrons transferred in metal deposition reaction

P_1 dimensionless parameter describing the relative importance of the backward term in the metal deposition reaction

P_2 dimensionless parameter describing the relative importance of the ohmic potential drop

P_3 dimensionless parameter describing the relative importance of the forward term in the side reaction

P_4 dimensionless parameter describing the relative rate of the backward term in the side reaction

P_5 dimensionless parameter which characterizes the ohmic potential drop in the pore-solution phase

P_6 dimensionless parameter which characterizes the ohmic potential drop in the matrix phase

R universal gas constant, 8.3143 J/mole-K

s_R stoichiometric coefficient of metal-ion reactant

T absolute temperature, K

UD upstream counterelectrode downstream current collector

UU upstream counterelectrode upstream current collector

U_j^θ standard electrode potential for reaction j , V

ΔU $= U_S - U_R$ difference in open-circuit cell potentials of the side reaction and primary reaction at the reference composition, V

v	superficial fluid velocity, cm/s
VOP	potential of the cathode current collector relative to a saturated calomel reference electrode placed in the dilute product stream, V
x	distance through porous electrode, cm
y	$x\, ak_m/v$ dimensionless distance through porous electrode
z_i	valance or charge number of species i

Greek letters

α	$= a\, k_m/v$, reciprocal of penetration depth at the limiting current, cm^{-1}
α_{aj}	anodic transfer coefficient for reaction j
α_{cj}	cathodic transfer coefficient for reaction j
ε	porosity or void volume
η	$= \Phi_1 - \Phi_2$ local overpotential, V
η'	dimensionless local overpotential, see equation 33
κ	effective conductivity of solution, mho/cm
σ	effective conductivity of solid matrix, mho/cm
Φ_1	electrostatic potential in matrix phase, V
Φ_2	quasi-electrostatic potential in the pore solution phase, V
θ	$= c_R/c_{Rf}$, dimensionless concentration of metal-ion reactant

Subscripts

R	metal-ion reactant or primary reaction
ref	reference composition
S	side reactant or side reaction

References

1. James A. Trainham and John Newman. "A Flow-Through Porous Electrode Model: Application to Metal-Ion Removal From Dilute Steams." Submitted to the Journal of the Electrochemical Society (Feb. 1977).

2. R. E. Sioda. "Current-Potential Dependence In the Flow Electrolysis on a Porous Electrode." Journal of Electroanalytical Chemistry and Interfacial Electrochemistry, 34, 399-409 (1972).

3. Richard Alkire and Brian Gracon. "Flow-Through Porous Electrodes." Journal of the Electrochemical Society, 122, 1594-1601 (1975).

4. Richard Alkire and Ronald Gould. "Analysis of Multiple Reaction Sequences in Flow-Through Porous Electrodes." Journal of the Electrochemical Society, 123, 1842-1849 (1976).

5. B. G. Ateya and L. G. Austin. "Steady-State Polarization at Flow-Through Electrodes with Small Pore Diameter I. Reversible Kinetics." Journal of the Electrochemical Society, 124, 83-89 (1977).

6. M. Paulin, D. Hutin, and F. Goeuret. "Theoretical and Experimental Study of Flow-Through Porous Electrodes." Journal of the Electrochemical Society, 124, 180-188 (1977).

7. P. V. Danckwerts. "Continuous Flow Systems. Distribution of Residence Times." Chemical Engineering Science, 2, 1-13 (1953).

8. J. F. Wehner and R. H. Wilhelm. "Boundary conditions of flow reactor." Chemical Engineering Science, 6, 89-93 (1956).

9. John Newman. Electrochmical Systems. Prentice-Hall Englewood Cliffs, N.J. (1973), Appendix C.

10. John Van Zee and John Newman. "Electrochemical Removal of Silver Ions from Photographic Fixing Solutions Using a Porous Flow-Through Electrode." Journal of the Electrochemical Society, 124, 706-708 (1977).

11. Douglas N. Bennion and John Newman. "Electrochemical removal of copper ions from very dilute solutions." Journal of Applied Electrochemistry, 2, 113-122 (1972).

12. James A. Trainham and John Newman. "A Thermodynamic Estimation of the Minimum Concentration Attainable in a Flow-Through Porous Electrode Reactor." Journal of Applied Electrochemistry, 7, (1977).

13. D. D. Wagman, W. H. Evans, V. B. Parker, I. Halow, S. M. Bailey and R. H. Schumm. "Selected Values of Chemical Thermodynamic Properties. Tables for the First Thirty-Four Elements in Standard Order of Arrangement." NBS Technical Note 270-3. Washington, D.C., National Bureau of Standards (1968) p. 47.

14. John A. Dean (editor). "Lange's Handbook of Chemistry." Eleventh edition, McGraw-Hill Book Company, New York (1973) p. 6-14.

15. John Newman and William Tiedemann. "Flow-Through Porous Electrodes." H. Gerischer and C. Tobias, ed., Advances in Electrochemistry and Electrochemical Engineering, 11, to be published.

16. John Newman. "Current Distribution on a Rotating Disk below the Limiting Current." Journal of the Electrochemical Society, 113, 1235-1241 (1966).

17. W. R. Parrish and John Newman. "Current Distribution on a Plane Electrode below the Limiting Current." Journal of the Electrochemical Society, 116, 169-172 (1969).

18. W. R. Parrish and John Newman. "Current Distributions on Plane, Parallel Electrodes in Channel Flow." Journal of the Electrochemical Society, 117, 43-48 (1970).

19. Limin Hsueh and John Newman. "The Approach to Limiting Current in a Stagnant Diffusion Cell." Journal of the Electrochemical Society, 117, 1242-1245 (1970).

TECHNICAL INFORMATION DIVISION
LAWRENCE BERKELEY LABORATORY
UNIVERSITY OF CALIFORNIA
BERKELEY, CALIFORNIA 94720